Proceedings of the 28th IEEE
EMBS Annual International Conference
New York City, USA, Aug 30-Sept 3, 2006

Analysis of Breathing Air Flow Patterns in Thermal Imaging

Jin Fei
Department of Computer Science
University of Houston
Houston, Texas 77204–3010
jinfei@cs.uh.edu

Ioannis Pavlidis
Department of Computer Science
University of Houston
Houston, Texas 77204–3010
ipavlidi@central.uh.edu

***Abstract*— We introduce a novel methodology to characterize breathing patterns based on thermal infrared imaging. We have retrofitted a Mid-Wave Infra-Red (MWIR) imaging system with a narrow band-pass filter in the CO_2 absorption band ($4130 - 4427\ nm$). We use this system to record the radiation information from within the breathing flow region. Based on this information we compute the mean dynamic thermal signal of breath. The breath signal is quasi-periodic due to the interleaving of high and low intensities corresponding to expirations and inspirations respectively. We sample the signal at a constant rate and then filter the high frequency noise due to tracking instability. We detect the breathing cycles through zero cross thresholding, which is insensitive to noise around the zero line. We normalize the breathing cycles and align them at the transition point from inhalation to exhalation. Then, we compute the mean breathing cycle. We use the first eight (8) harmonic components of the mean cycle to characterize the breathing pattern. The harmonic analysis highlights the intra-individual similarity of breathing patterns. Our method opens the way for desktop, unobtrusive monitoring of human respiration and may find widespread applications in clinical studies of chronic ailments. It also brings up the intriguing possibility of using breathing patterns as a novel biometric.**

I. Introduction

Many respiratory diseases like sleep apnea syndrome and bronchial asthma are common in clinical practice. Abboud *et al.* [1] and Howson *et al.* [2] reported the association of chronic obstructive lung diseases with characteristic respiratory flow waveforms. Even in the absence of pathophysiological causes, pattern analysis reveals that individual breathing patterns are not random [3]. Therefore, breathing patterns are important indicators of health status and individuality. Methods to sense and analyze breathing patterns have found many applications in medicine and may find some applications in biometrics.

So far, most studies of individual breathing patterns have been carried out using contact sensing. In these studies the breathing pattern is typically characterized by inspiratory phase duration (T_I), expiratory phase duration (T_E), and tidal volume (V_T). Clark *et al.* [4] and Cunningham *et al.* [5] studied breathing patterns based on T_I and T_E. Shea *et al.* [6] performed two studies on respiratory variables T_I, T_E, and V_T through pneumotachometer and respiratory inductance plethysmography. In [7] [8], Benchetrit *et al.* measured T_I, T_E, V_T and other air flow variables through a pneumotachometer. They quantified the shape of the breathing profile by the first four harmonics of Fourier transform.

Hämäläinen *et al.* [9] suggested optimal control modeling to predict various patterns of spontaneous breathing. The lung-ribcage mechanical system was approximated by a first order linear differential equation according to two criteria:

1) Minimize the change of lung volume at the beginning of inspiration and at the end of expiration;
2) Reach the tidal volume at the end of inspiration.

The discovery of similar breathing patterns in twins signified the role of genetics in brain stem respiratory rhythm generation [6][10]. Each person appears to have a characteristic breathing pattern. This might be explained by chemical feedback loops from the central nervous system [3].

Existing contact sensing for breathing pattern analysis requires the subject's cooperation. Novel non-contact means of sensing breath have enormous potential in monitoring respiratory diseases. They are more convenient to patients when used on a prolonged basis and are far more appropriate for neonates [11]. The potential benefit can be immediately realized by looking at Fig. 1, which depicts the standard wiring of a patient under monitoring for diagnosis of a chronic respiratory disease.

Thermal infrared imaging is a passive non-contact modality, which was proved successful in measuring breathing rate [12][13]. However, it is the first time that thermal infrared imaging is used for analysis of the breathing flow profile.

Fig. 1. Patient outfit during pulmonary studies. The chest straps and electronics are being used to record the breathing signal.

Occasional irregularities in the amplitude, rate, and general pattern of breathing are the major challenges to obtain a representative breath cycle [14]. To tackle these problems, we manipulate the thermal breathing signal via two-way normalization. Then, we perform harmonic analysis on the normalized signal to characterize the human breathing pattern. The major highlights of our work are:

- Use of a highly sensitive thermal imaging system with appropriate optical filtering to acquire the breathing signal;
- Low-pass filter design to reduce signal noise;
- piecewise monotone interpolation to normalize the breathing cycle;
- Harmonic analysis to parameterize the breathing pattern;
- Identifying the potential of breathing pattern as a biometric signature.

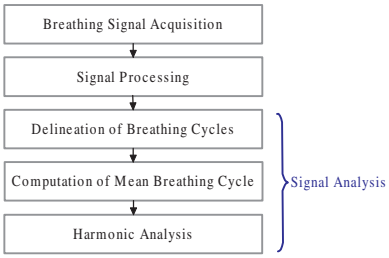

Fig. 2. Outline of our breathing pattern analysis methodology.

Fig. 2 outlines our methodology. Its basic components are breathing signal acquisition and processing as well as analysis. Section II describes our signal acquisition and processing method. In section III, we explain our breathing signal analysis method, which is based on breathing cycle alignment and harmonic analysis. We discuss our experimental setup and results in sections IV. Section V concludes the paper.

II. Signal Acquisition and Processing

The first part of our method is signal acquisition and processing. We explain the thermal radiation properties of breath through an optical band-pass filter tuned to the CO_2 absorption band ($4130 - 4427\ nm$). These properties are critical to our acquisition method. Then, we describe the region of interest selection in the thermal imagery, as well as the re-sampling and filtering of the breathing signal.

A. Signal Acquisition

Radiation refers to the continuous emission of energy from a surface. Radiation emission is described by Planck's Blackbody Law:

$$M(\lambda, T) = \frac{c_1}{\lambda^5}\left(\frac{1}{e^{(\frac{c_2}{\lambda T})} - 1}\right), \quad (1)$$

where $c_1 = 3.7411 \times 10^8 W * \mu m^4/m^2$, $c_2 = 1.4388 \times 10^4 \mu m * K$, λ is the wavelength in μm, and T is the surface temperature in Kelvin.

A thermal infrared camera senses the radiation that emanates from the scene [15]. We use a MWIR camera, which is sensitive to $3000 - 5000\ nm$ wavelength region. By integrating Equation (1) across these wavelengths we can approximate the amount of radiation sensed by the MWIR system:

$$M(\triangle\lambda, T) = \int_{\lambda_1}^{\lambda_2} M(\lambda, T) d\lambda, \quad (2)$$

where $\lambda_1 = 3000\ nm$ and $\lambda_2 = 5000\ nm$. In fact, because we use a narrow band-pass filter in the CO_2 absorption zone the integration range is much tighter ($\lambda_1 = 4130\ nm$ and $\lambda_2 = 4427\ nm$).

Equation (2) demonstrates that there is a direct connection between object temperatures in the scene and intensity levels in the thermal imagery. The expired air has temperature close to the core temperature of the body ('hot'). Therefore, the Focal Plane Array (FPA) of the MWIR imaging system senses higher radiation intensity in the expired airflow of a typical scene. The expired air is also rich in CO_2. Since the filter allows only radiation in the CO_2 absorption zone to reach the FPA, the contrast between the expired air and the background (e.g., wall) is strengthened, due to the prevalence of the greenhouse effect. During inspiration, the majority of the radiation in the breath air flow region is from the background ('cold'). Consequently, the FPA senses lower levels of radiation in the region of interest. In other words, the radiation of human breathing is quasi-periodic due to the interleaving of high and low radiation intensities corresponding to 'hot' expirations and 'cold' inspirations respectively.

B. Signal Processing

All the subjects in our video clips are mostly stationary and exhibit occasional minor head movement. Although the displacement of the head is small compared to the size of the image, it still introduces an error. To minimize motion errors, we use a tracking algorithm [16].

We select as the Measurement Region of Interest (MROI) an area just below the tip of the nose and up to the level of the mouth, where we expect the expired stream of air to flow through (see Fig. 3). We compute the mean temperature within the MROI in each frame. Along the timeline, this produces a quasi-periodic temperature signal, which is indicative of the breathing function.

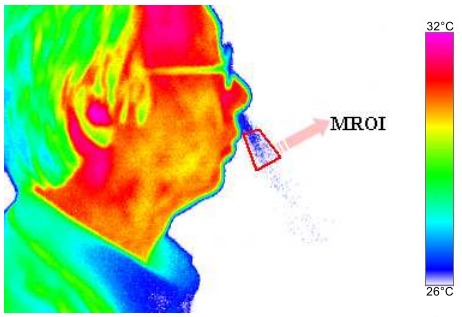

(a) (b)

Fig. 3. Thermal image of breathing: (a) the Measurement Region of Interest (MROI) is depicted as a polygon next to the nasal-mandibular region; (b) temperature color-map.

The video sampling rate fluctuates around 55 frames per second (fps). A constant sampling rate is necessary. We chose 10 fps as the re-sampling rate of the temperature signal. Since the mean breathing rate of a human being is between $0.2 - 0.3\ Hz$ [17], our re-sampling rate is more

than enough ($10 \gg 0.3$) to reconstruct the breathing signal without information loss (Nyquist theorem).

The tracker's imperfections and occasional instability introduce a high frequency noise component into the thermal breathing signal. We use a low-pass filter to reduce this high frequency component. Specifically, we use the Butterworth digital filter [18], which is one of the most commonly used filters in digital signal processing. Its main advantages are that it is fast and simple. The amplitude response of a Butterworth filter is maximally flat in the pass band and monotonic overall. The detailed specification of the Butterworth filter we use is as follows: its order is $n = 10$, its pass-band frequency range is $[0, 1]\ Hz$ (to allow up to the 8-th harmonic component), and its 60 dB attenuation stop-band frequency is 2 Hz. The amplitude response of our filter is shown in Fig. 4.

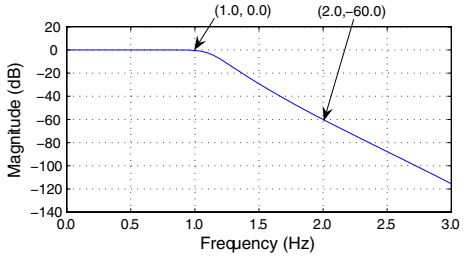

Fig. 4. The frequency response of our Butterworth digital filter.

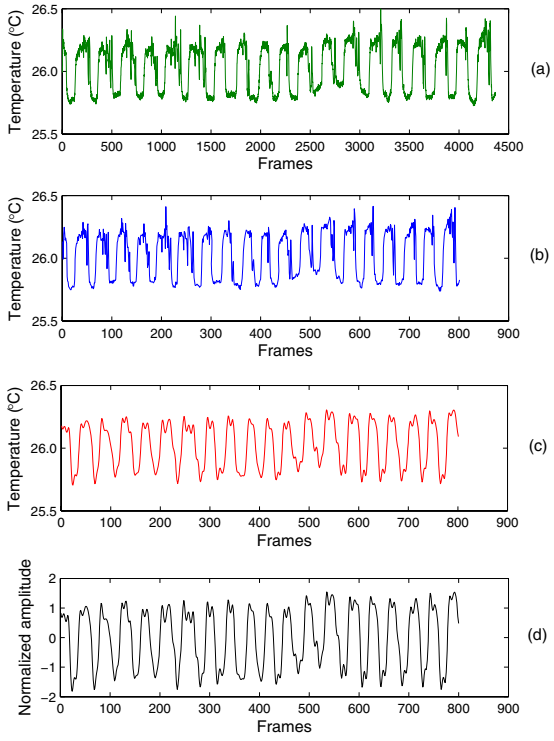

Fig. 5. Signal processing of the thermal breathing signal: (a) Original thermal breathing signal in MROI expressed in $^{\circ}C$; (b) Re-sampled breathing signal; (c) Filtered breathing signal (Butterworth filter); (d) Normalized signal that has mean amplitude 0 and standard deviation 1.

We define as $V(t),\ t \in \{0, \cdots, N\}$, the filtered thermal breathing signal. We normalize the signal amplitude as follows:

$$V'(t) = \frac{V(t) - \mu}{\sigma}, \tag{3}$$

where μ and σ are the mean and standard deviation of $V(t)$ respectively. The normalization transforms signal $V(t)$ to $V'(t)$ that features mean $\mu' = 0$ and standard deviation $\sigma' = 1$.

In Fig. 5, we illustrate the results of re-sampling, low-pass digital filtering, and amplitude normalization.

III. Signal Analysis

Breathing is a rhythmic phenomenon characterized by the repetition of inspiration and expiration. In this section, we outline the methodology we apply on the pre-processed thermal signal to delineate and analyze the breathing cycles.

A. Delineation of Breathing Cycles

We perform zero cross thresholding to achieve robust breathing cycle delineation. Fig. 6 depicts an example of a pre-processed thermal breathing signal. The dashed black line is the zero cross line. In zero cross thresholding, this line is typically bounded by two adjustable thresholds above and below. In our case, we chose the two adjustable thresholds to be 20% of the maximum signal amplitude on either side of the zero cross line. The corresponding time frames when the signal reaches and leaves the thresholds are defined as 'Zero Cross Start' and 'Zero Cross End' respectively. We average these two time frames to obtain the effective 'Zero Cross' time frame. This threshold strategy is less sensitive to small signal fluctuations around the zero cross line. Such noisy fluctuations may result into spurious breathing cycles and adversely affect the breathing signal analysis.

Zero cross thresholding minimizes, but does not eradicate faulty cycle starts. Specifically, we define as normal cycles those that start with a Positive Sub-Cycle (PSC) and end with a Negative Sub-Cycle (NSC). The rationale for our convention is that it is less prone to error to detect transitions from inspiration to expiration, because they are sharper (muscular contraction) than transitions from expiration to inspiration (passive process) [17]. Based on our convention, cycles that start with NSC are faulty. There is an example of such a faulty start, which is not caught by zero cross thresholding in Fig. 6. A heuristic approach to address this problem is to accept a cycle as legitimate if it starts with PSC and ignore cycle parts that start with NSC.

B. Computation of Mean Breathing Cycle

Cycles in a breathing waveform vary in shape and duration. We have already normalized the breathing cycles in terms of amplitude (see section II). In order to compute the mean cycle of a breathing waveform, we also need to normalize the cycles in terms of duration. We perform a piecewise cubic interpolation (Hermite) [19] on the breathing cycles that preserves monotonicity and shape. Each breathing cycle is mapped to an iso-distant sequence of 128 points.

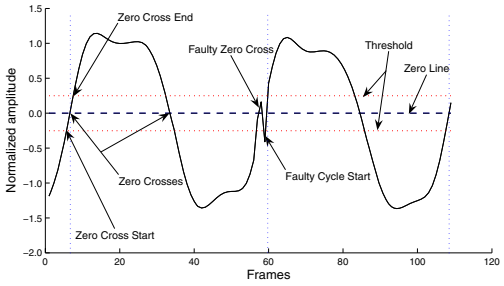

Fig. 6. Breathing cycle delineation: the dashed blue vertical lines separate each cycle; the dashed black horizontal line is the zero cross line; the two dashed red horizontal lines define the thresholds.

Since the data sequence of the original cycle contains typically much fewer points than 128, the interpolation also improves the smoothness of the curve. Fig. 7 shows the interpolation of a breathing cycle curve with 35 discrete points $(35 * 0.1 = 3.5\ sec)$ to the standard sequence of 128 points.

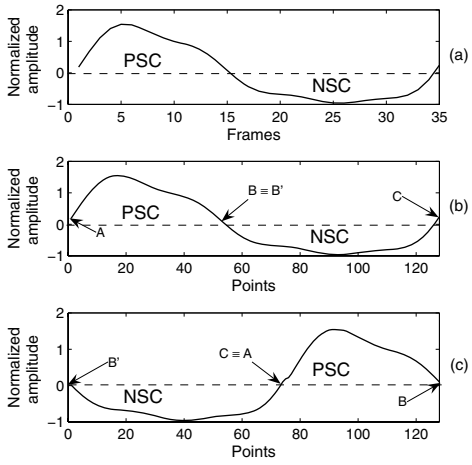

Fig. 7. (a) Mean breathing cycle of 35 points (3.5 sec). (b) The mean breathing cycle after monotone piecewise interpolation. (c) Shift of the NSC and PSC portions of the cycle.

If after the two-way normalization (amplitude and duration) we attempt to compute the mean breathing cycle we will introduce significant distortion at the transition point from PSC to NSC [8]. The PSC and NSC components of each cycle are not fully symmetrical. Therefore, it is better to align the cycles at the transition point instead of the two end points. We shift the NSC component of each cycle to align it at the beginning of PSC. The end of NSC anneals with the beginning of PSC. This shift preserves the periodicity of the breathing cycle (see Fig. 7 (c)). In Fig. 8, 50 cycles of a breathing waveform are normalized, shifted, and aligned at the transition point. The computed mean breathing cycle shows as a thick solid yellow curve.

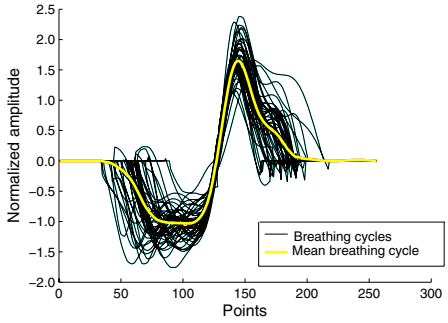

Fig. 8. Computation of the mean breathing cycle out of 50 cycles of a breathing waveform.

C. Harmonic Analysis

Harmonic analysis breaks a signal into characteristic components that can serve as pattern descriptors. We typically perform harmonic analysis through Fourier transformation. We apply the Fast Fourier Transform (FFT) [20] on the mean breathing cycle $\bar{V}'(k), k \in \{0, \cdots, N-1\}$, to compute its harmonic components $X(n)$:

$$X(n) = \sum_{k=0}^{N-1} \bar{V}'(k) e^{-\frac{i2\pi nk}{N}}, n \in 0, \cdots, N-1 \qquad (4)$$

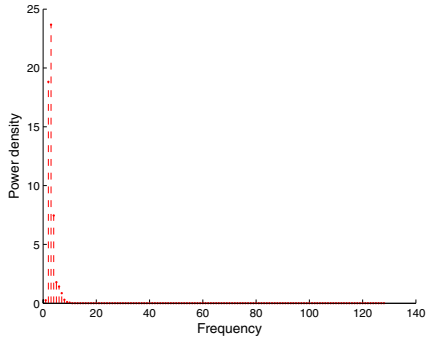

Fig. 9. Power density spectrum of the mean breathing cycle of a subject.

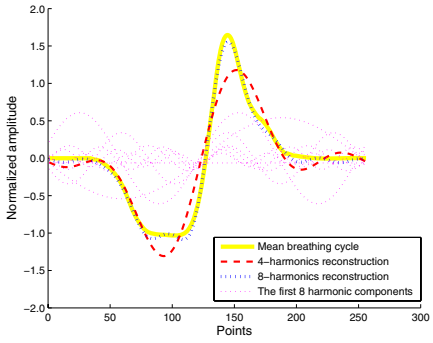

Fig. 10. Mean breathing signal reconstruction from the first 4 and 8 harmonics.

Breathing is a low frequency phenomenon and we capitalize on this in harmonic analysis. Indeed, Fig. 9 shows that the

power density of the mean breathing cycle of a subject is typically concentrated in the low frequency range. Therefore, the first few harmonics can effectively characterize the shape of the mean breathing cycle. We have found experimentally that the first 8 harmonics carry sufficient reconstructing power and can fully represent the shape of the signal. Fig. 10 shows the original mean breathing signal of a subject along with the first 8 harmonics and signal reconstructions based on 4 and all 8 harmonics. It is evident that the signal reconstruction based on 4 harmonics cannot reproduce exactly the original shape and there is some loss of information. By contrast the signal reconstruction based on 8 harmonics is perfect.

IV. Experimentation

A. Experimental Setup

The center-piece of the imaging system we used in our experiments is a Flir Phoenix Mid-Wave Infra-Red (MWIR) camera with an Indium Antimonite (InSb) detector operating in the range $3000 - 5000\ nm$ [21]. The camera has a focal plane array (FPA) with maximum resolution of 640×512 pixels and a maximum sampling rate of $120\ fps$. The sensitivity is $0.025^{\circ}\ C$. The camera was outfitted with a MWIR $50mm$ lens $f/2.3$, $Si : Ge$, bayonet mount from Flir Systems [21].

A narrow band-pass optical filter (4130-4427 nm) from Spectrogon [22] was attached between the camera's FPA and lens. The mean wavelength of the filter is $\mu_f = 4269\ nm$, which is close to the absorption wavelength of the fundamental vibration of CO_2 molecules.

Subjects were located $6 - 8\ ft$ away from the imaging system and offered a profile view. The experiments took place in a dimly lit, climate controlled room. The MWIR camera was calibrated with a two-point calibration at $28^{\circ}\ C$ and $38^{\circ}\ C$, which are the end points of a typical temperature distribution on a subject's face. The mean video recording speed was set at $55\ fps$.

B. Experimental Results

We recorded eleven (11) thermal clips from five (5) healthy subjects at rest. For four (4) of the subjects we recorded two (2) clips on different days (about two weeks apart). For one (1) of the subjects we recorded three (3) clips, two (2) of which were done on the same day. All thermal clips are about $5\ min$ in duration.

We applied on the video clips of all the subjects ($S1 - S5$) the processing and analysis methodology outlined in sections II-B - III. Fig. 11 depicts the resulting mean breathing cycles and harmonic components. Specifically, each of Fig. 11 (a)-(e) consists of two graphs. The top graph shows the mean breathing cycles for a subject on two *different* days. The bottom graph shows the first 8 harmonic components of the two curves depicted on the top graph. Fig. 11 (f) shows the mean breathing cycles and harmonic components of recordings done for subject $S5$ on the *same* day. We symbolize as $Sx.1$ and $Sx.2$ or $Sx.3$ the mean breathing cycles computed for subject Sx on recordings done on 02-08-2005 and 02-23-2005 respectively. We also denote as $Sx.y.n$ the n-th harmonic component of curve $Sx.y$, where $x \in \{1, 2, \ldots, 5\},\ \ y \in \{1, 2, 3\},$ and $n \in \{1, 2, \ldots, 8\}$.

From Fig. 11 we can observe that the mean breathing cycle curves for the same subject on different days (or the same day) are very similar. There is indication that the intra-individual breathing pattern remains consistent over time. Regarding the harmonic components, the fundamental component contains only a real part and does not affect the shape of the cycle. The rest of the harmonics have both real and imaginary parts. As Fig. 11 shows, harmonic components $n = 2, 3, 4$ are away from the origin and dominate the shape of the curve. The harmonic components $n = 5, 6, 7, 8$ contribute only to shape detail.

It has been suggested in the literature that inter-individual breathing patterns are mostly dissimilar [3]. These legacy studies were performed with contact sensing means. To investigate this issue further using our novel contact-free sensing methodology, we compute the Euclidean distances between the harmonics that define the mean breathing cycles depicted in Fig. 11. Table I lists intra-individual and inter-individual distances of harmonic sets for all subjects. The general trend revealed from the data is that intra-individual differences are smaller than inter-individual differences. For instance, subject $S1$ has intra-individual harmonic distance $d_{11} = 19.93$, which is smaller than any inter-individual distance between this subject and any other subject. There are a few exceptions to this trend. For example, subject $S2$ has intra-individual harmonic distance $d_{22} = 29.19$, which is larger than its inter-individual harmonic distances from subject $S3$ (25.60 and 18.66) in one of the recordings. To facilitate readability, intra-individual distances are typed in bold face and inter-individual distances that are against the trend are typed in italics.

Fig. 12 shows the Cumulative Math Characteristic Curve (CMC), which indicates the potential of the breathing pattern as a biometric signature. If the candidate list contains only the smallest distance, in 64% of the cases this belongs to an intra-individual measurement. If the candidate list contains the four (4) smallest distances, in 100% of the cases there is an intra-individual measurement among them.

The analysis of the experimental results indicates that intra-individual breathing patterns remain consistent over time and can be used to characterize normalcy. Due to the contact-free and highly automated nature of the method this may find widespread applications in medical studies of respiratory abnormalities with stochastic appearance. Examples of such abnormalities are asthma, chronic bronchitis, and obstructive sleep apnea. The imaging system can be mounted on the desktop or over the bed and monitor the subject passively for long periods that last several minutes or hours, without disrupting his/her office or sleep routine. The use of an effective facial tissue tracker (as the one used in our system) appears to adequately address natural head motion.

The results also indicate that there is a degree of uniqueness in the breathing pattern that can be used as a biometric signature. However, the data set is small to extract any solid conclusion other than that the problem merits more study.

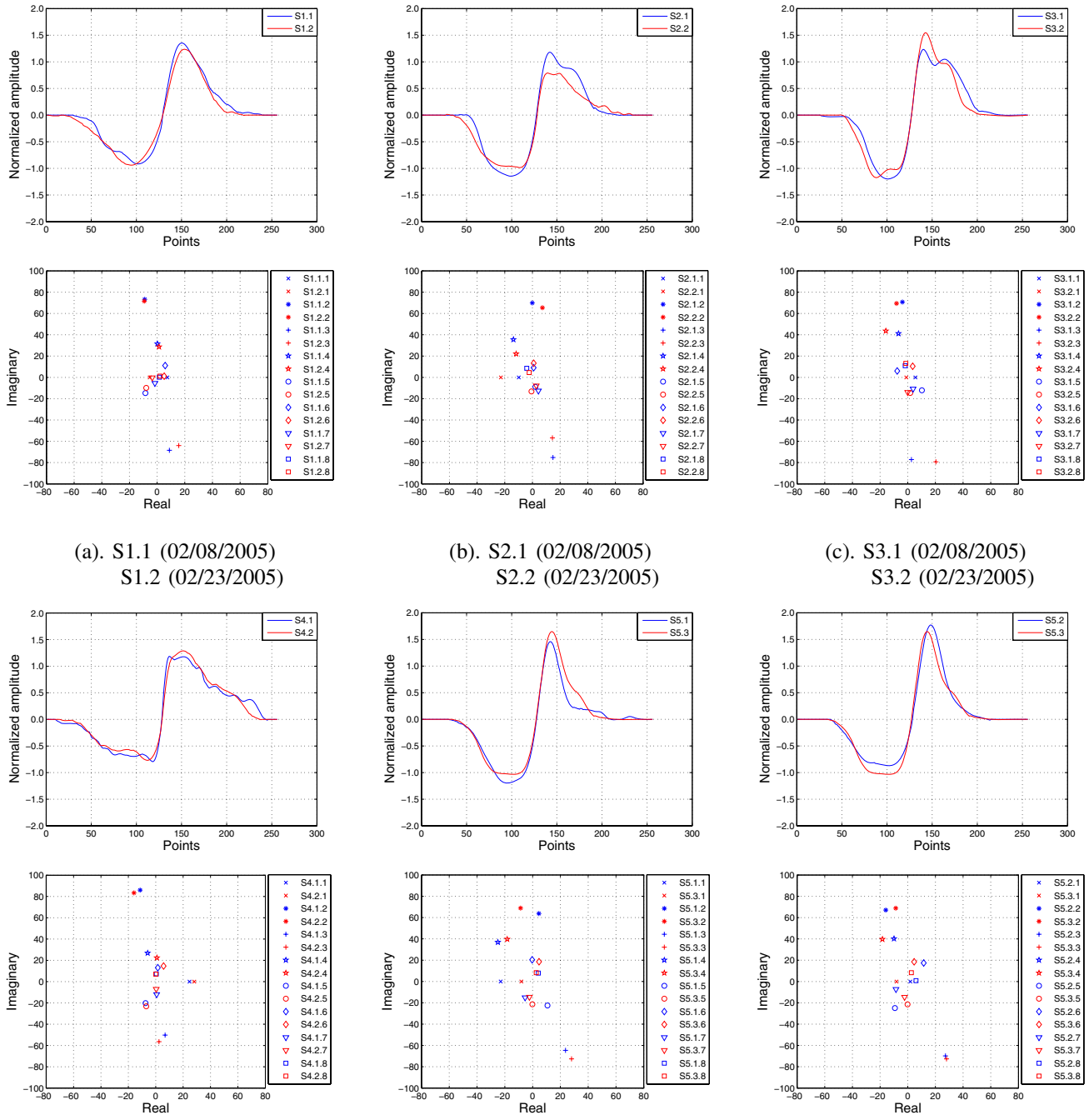

(a). S1.1 (02/08/2005) S1.2 (02/23/2005)

(b). S2.1 (02/08/2005) S2.2 (02/23/2005)

(c). S3.1 (02/08/2005) S3.2 (02/23/2005)

(d). S4.1 (02/08/2005) S4.2 (02/23/2005)

(e). S5.1 (02/08/2005) S5.3 (02/23/2005)

(f). S5.2 (02/23/2005) S5.3 (02/23/2005)

Fig. 11. Shape and harmonics of mean breathing cycle. In each of (a)-(f): the top graph shows the mean breathing cycles of two recordings for a subject; the bottom graph shows the corresponding first 8 harmonic components of the two curves.

V. Conclusion

In this paper, we demonstrated that the acquisition and analysis of the breathing signal are possible using thermal infrared imaging. The methodology is passive, contact free, and highly automated. This means that it can be safely employed to monitor patients at home or the office for long periods of time.

We managed to acquire a breathing signal with sufficient Signal to Noise (S/N) ratio by outfitting a highly sensitive MWIR camera with a narrow band-pass optical filter in the CO_2 absorption zone. After signal processing, which included normalization of amplitude and duration, we were able to compute the mean breathing cycle of a breathing waveform. Then, we quantified the shape of the mean breathing cycle in terms of the first 8 harmonics.

TABLE I

EUCLIDEAN DISTANCES OF HARMONIC SETS

Subjects	Clips	Subject 1		Subject 2		Subject 3		Subject 4		Subject 5		
		S1.1	S1.2	S2.1	S2.2	S3.1	S3.2	S4.1	S4.2	S5.1	S5.2	S5.3
1	S1.1	0.00	**19.93**	32.33	42.29	32.28	33.16	31.85	31.48	53.12	29.70	37.10
	S1.2	**19.93**	0.00	31.61	35.22	38.84	36.83	43.58	45.16	50.70	34.22	38.84
2	S2.1	32.33	31.61	0.00	**29.19**	***25.60***	***18.66***	51.75	56.35	33.29	39.24	***25.61***
	S2.2	42.29	35.22	**29.19**	0.00	46.80	43.36	57.58	62.77	31.45	48.58	38.54
3	S3.1	32.28	38.84	***25.60***	46.80	0.00	**26.85**	46.36	48.67	49.00	47.02	39.91
	S3.2	33.16	36.83	***18.66***	43.36	**26.85**	0.00	50.22	54.18	37.02	30.32	***18.33***
4	S4.1	31.85	43.58	51.75	57.58	46.36	50.22	0.00	**14.73**	66.54	47.09	52.56
	S4.2	31.48	45.16	56.35	62.77	48.67	54.18	**14.73**	0.00	72.86	48.86	57.45
5	S5.1	53.12	50.70	33.29	31.45	49.00	37.02	66.54	72.86	0.00	44.73	**26.76**
	S5.2	29.70	34.22	39.24	48.58	47.02	30.32	47.09	48.86	44.73	0.00	**23.17**
	S5.3	37.10	38.84	25.61	38.54	39.91	***18.33***	52.56	57.45	**26.76**	**23.17**	0.00

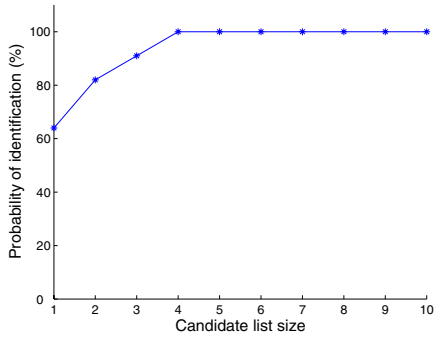

Fig. 12. Cumulative Math Characteristic (CMC) curve.

The analysis of the experimental results indicates that the pattern of breathing, as expressed by the mean breathing cycle, is remarkably consistent for the same individual over time. Therefore, abnormalities in the individual patterns can be easily spotted.

Our research demonstrates the feasibility of this new technology and opens the way for clinical studies. The results also indicate the potential use of breathing pattern as a biometric signature, although further research and experiments are required to establish the feasibility of this idea.

ACKNOWLEDGEMENTS

This research is part of the Interacting with Human Physiology project funded by the National Science Foundation (grant #IIS-0414754). The views expressed by the authors in this paper do not necessarily reflect the views of the funding agency. Special thanks to Jonathan Dowdall from the Computational Physiology Lab at the University of Houston for his invaluable tracking algorithms.

REFERENCES

[1] S. Abboud, I. Bruderman, and D. Sadeh, "Frequency and time domain analysis of airflow breath patterns in patients with chronic obstructive airway disease," *Comput Biomed Res*, vol. 19, p. 266273, 1986.

[2] M. Howson, S. Khamnei, D. OConnor, and P. Robbins, "The properties of a turbine device for measuring respiratory," *volumes in man. J Physiol (Lond)*, vol. 382, p. 12, 1986.

[3] G. Benchetrit, "Breathing pattern in humans: Diversity and individuality," *Respiration Physiology*, vol. 122, pp. 123–9, Sep 2000.

[4] F. J. Clark and C. von Euler, "On the regulation of depth and rate of breathing," *Journal of Physiology*, pp. 222–267, 1972.

[5] D. Cunningham and W. N. Gardner, "A quantitative description of the pattern of breathing during steady-state co_2 inhalation in man, with special emphasis on expiration," *Journal of Physiology*, pp. 272–613, 1977.

[6] S. Shea, G. Benchetrit, D. T. Pham, R. Hamilton, and A. Guz, "The breathing patterns of identical twins," *Respiration Physiology*, vol. 75, pp. 211–23, Feb 1989.

[7] J. P. Bachy, A. Eberhard, P. Baconnier, and G. Benchetrit, "A program for cycle-by-cycle shape analysis of biological rhythms - Application to respiratory rhythm," *Computer Methods and Programs in Biomedicine*, vol. 23, pp. 297–307, 1983.

[8] G. Benchetrit, S. Shea, D. T. Pham, S. Bodocco, P. Baconnier, and A. Guz, "Individuality of breathing patterns in adults assessed over time," *Respiration Physiology*, vol. 75, pp. 199–209, Feb 1989.

[9] R. Hämäläinen and A. Viljanen, "Modelling the respiratory airflow pattern by optimization criteria," *Biol. Cybern.*, vol. 29, pp. 143–149, 1978.

[10] J. Changeux, *Neuronal man : the biology of mind*. New York : Pantheon Books, 1985. pp 205-249.

[11] S. A. Kharitonov and P. J. Barnes, "Exhaled markers of pulmonary disease," *Am. J. Respir. Crit. Care Med.*, vol. 163, pp. 1693–1722, June 2001.

[12] J. Fei, Z. Zhu, and I. Pavlidis, "Imaging breathing rate in the co_2 absorption band," in *Proceedings of the 27th Annual International Conference IEEE Engineering in Medicine and Biology Society*, (Shanghai, China), September 1-4 2005.

[13] R. Murthy, I. Pavlidis, and P. Tsiamyrtzis, "Touchless monitoring of breathing function," in *Proceedings of the 26th Annual International Conference IEEE Engineering in Medicine and Biology Society*, (San Fransisco, CA), September 2004.

[14] J. Sato and P. Robbins, "Methods for averaging irregular respiratory flow profiles in awake humans," *Journal of Applied Physiology*, vol. 90, pp. 705–712, 2001.

[15] G. C. Holst, *Common Sense Approach to Thermal Imaging*, ch. 5. Bellingham, Washington: SPIE-The International Society for Optical Engineering, 2000.

[16] P. Tsiamyrtzis, J. Dowdall, D. Shastri, I. Pavlidis, M. Frank, and P. Eckman, "Lie detection - recovery of the periorbital signal through tandem tracking and noise suppression in thermal facial video," in *Proceedings of the SPIE Sensor, and Command, Control, Communications, and Intelligence Technologies for Homeland Security and Homeland Defense IV* (E. Carapezza, ed.), vol. 5778, (Orlando, Florida), March 27-30 2005.

[17] F. H. Martini, W. C. Ober, C. W. Garrison, K. Welch, and R. T. Hutchings, *Fundamentals of Anatomy and Physiology*, ch. 23. Upper Saddle River, N.J.: Prentice Hall, 5th ed., 2001.

[18] L. Rabiner and B. Gold, *Theory and Application of Digital Signal Processing*. NJ:Prentice-Hall, 1975. pg. 227.

[19] F. Fritsch and R. Carlson, "Monotone piecewise cubic interpolation," *SIAM J. Numer. Anal.*, vol. 2, pp. 238–246, 1980.

[20] J. Cooley and J. Tukey, "An algorithm for the machine computation of the complex fourier series," *Mathematics of Computation*, vol. 19, pp. 297–301, April 1965.

[21] FLIR Systems Inc., 27700A SW Parkway Avenue, Wilsonville, Oregon 97070, *http://www.flirsystems.com*.

[22] Spectrogon US Inc., 24B Hill Road, Parsippany, New Jersey 07054, *http://www.spectrogon.com*.